Reactive Ballistic Deposition of α-Fe_2O_3 Thin Films for Photoelectrochemical Water Oxidation

Nathan T. Hahn,[†] Heechang Ye,[‡] David W. Flaherty,[†] Allen J. Bard,[‡] and C. Buddie Mullins[†,‡,*]

[†]Department of Chemical Engineering, Texas Materials Institute, Center for Nano- and Molecular Science, The University of Texas at Austin, 1 University Station C0400, Austin, Texas 78712 and [‡]Center for Electrochemistry, Department of Chemistry and Biochemistry, The University of Texas at Austin, 1 University Station A5300, Austin, Texas 78712

ABSTRACT We report the preparation of α-Fe_2O_3 electrodes using a technique known as reactive ballistic deposition in which iron metal is evaporatively deposited in an oxygen ambient for photoelectrochemical (PEC) water oxidation. By manipulating synthesis parameters such as deposition angle, film thickness, and annealing temperature, we find that it is possible to optimize the structural and morphological properties of such films in order to improve their PEC efficiency. Incident photon to current conversion efficiencies (IPCE) are used to calculate an AM1.5 photocurrent of 0.55 mA/cm^2 for optimized films with an IPCE reaching 10% at 420 nm in 1 M KOH at +0.5 V *versus* Ag/AgCl. We also note that the commonly observed low photoactivity of extremely thin hematite films on fluorine-doped tin oxide substrates may be improved by modification of annealing conditions in some cases.

KEYWORDS: hematite · photocatalysis · water splitting · solar · nanostructured

Efficient solar driven hydrogen production using cheap, stable materials has been an ambitious dream for several decades, with an explosion of study originating with the suggestion of water splitting in a Pt-TiO_2 electrochemical cell in the early 1970s.[1] Due to the recent ecological and energy crises related to fossil fuel dependence, such avenues for solar energy conversion have once again been thrust into the public view,[2] and research efforts along these lines are accelerating throughout the world, with a recent emphasis on the development of novel, nanostructured materials for hydrogen production through photoelectrochemical water splitting. Due to the difficulty of discovering a single semiconductor that can simultaneously produce oxygen and hydrogen from water, a common approach is to develop and optimize semiconductor materials for the oxidation and reduction steps of the water splitting reaction independently. In this work, we employ a new technique known as reactive ballistic deposition[3−6] to prepare and optimize nanostructured α-Fe_2O_3 films for the photo-oxidation of water.

In recent years a number of groups have investigated thin films consisting of vertically oriented nanocolumnar structures, which are thought to be ideal for photoelectrochemical water splitting due to their ability to absorb a significant fraction of light while still providing short charge carrier transport distances to the electrolyte, minimizing recombination losses.[7] For example, extensive research has been performed on TiO_2 nanotube arrays produced by electrochemical anodization, and impressive photoconversion efficiencies have been obtained, indicating that such architectures are quite useful for the photo-oxidation of water under UV irradiation.[8,9] However, to achieve necessary solar-to-hydrogen conversion efficiencies of more than 10%,[10] materials with the ability to absorb a good fraction of the visible light spectrum (>400 nm) are needed. Hematite (α-Fe_2O_3) was introduced as a PEC material over 30 years ago, and its 2.2 eV band gap theoretically suggests that it can achieve a maximum photoconversion efficiency under solar illumination of 12.9%.[11] However, the best performing thin film materials developed to date fall well short of this value.[12] This is attributed to a number of factors, including poor mobility of carriers, slow water oxidation kinetics, and high recombination rates compared to other semiconductors of interest such as TiO_2 and WO_3.[13] The means of improving photocurrent response in α-Fe_2O_3 films are essentially directed at aiding charge transport in the bulk and at the surface relative to recombination in both locations. Manipulation of preparation conditions in order to optimize film properties such as morphology and crystallinity can improve rates of charge transport in the bulk, while the

*Address correspondence to mullins@che.utexas.edu.

Received for review January 6, 2010 and accepted March 24, 2010.

Published online April 2, 2010.
10.1021/nn100032y

addition of a cocatalyst to the surface of the film can improve heterogeneous charge transfer kinetics. Doping foreign elements into α-Fe_2O_3 films can also be used to achieve similar improvements. Elements such as Si,[12] Ti,[14] Sn,[15] Pt,[16] and others have shown the ability to increase the photoelectrochemical performance of hematite films. The use of multiple dopants simultaneously has also been investigated with some success.[15,17] For this reason, there is still hope for α-Fe_2O_3-based materials in the field of photoelectrochemical water splitting, and there has been a recent surge of activity in the preparation of such thin films by techniques including spray pyrolysis,[17−19] chemical vapor deposition (CVD),[12,20] electrodeposition,[21,22] and electrochemical anodization.[23,24]

One technique that has received some recent attention for photoelectrochemical applications is glancing or oblique angle deposition (GLAD or OAD).[25] The method employs a ballistic shadowing phenomenon, which occurs when a material is directionally deposited onto a relatively cool substrate at glancing angles. The initial roughening of the substrate surface caused by random variations in the local deposition rate results in small agglomerates of atoms, which begin to intercept greater and greater amounts of depositing material and shadow other regions of the surface. As this process continues, these deposits of atoms begin to form nanocolumnar structures with characteristic dimensions that depend on the deposition angle and substrate temperature used. By increasing the angle between evaporant flux and substrate surface normal (deposition angle), the films become more porous and eventually form individual nanocolumns. A number of groups have characterized this technique extensively, applying it to materials such as TiO_2,[26] MgF_2,[27] indium tin oxide (ITO),[28] and Pd.[29] GLAD techniques carried out *via* the directional evaporation of a metal component in an ambient reactive gas are known as reactive ballistic deposition[3] (RBD) and can be used to control both composition and morphology independently. However, to our knowledge, no work has been done to characterize its efficacy for producing thin films for efficient photoelectrochemistry, although recently groups have used GLAD to evaporate TiO_2[30] and ZnO,[31] producing nanostructured electrodes for water splitting applications. In this work, we utilize RBD to prepare undoped α-Fe_2O_3 films, with the ultimate goal of understanding how this method may be applied to the synthesis of useful PEC materials.

RESULTS AND DISCUSSION

General Characterization. Immediately following synthesis, the films appeared dark brown, but upon annealing for 2 h at temperatures greater than 400 °C, the color of the films changed to reddish orange. Energy dispersive X-ray spectroscopy (EDS) performed prior to annealing reveal that the Fe/O ratio is already 2:3 after removing the samples from the vacuum chamber. X-ray diffraction (XRD) performed on films as-deposited showed no noticeable hematite (α-Fe_2O_3) formation, revealing only the presence of a small amount of maghemite (γ-Fe_2O_3), indicating that the films are mostly amorphous before annealing. After annealing, XRD shows the presence of α-Fe_2O_3 with a preferred (104) orientation, consistent with powder standards (PDF #01-071-5088; Figure 1), although some amorphous iron oxide most likely remains in the film. No other peaks other than those belonging to the fluorine-doped tin oxide (FTO) substrate can be observed. X-ray photoelectron spectroscopy (XPS) confirms that the films consist of Fe_2O_3 after annealing (Figure S1 in Supporting Information). UV−vis transmission experiments performed on annealed films show an absorption onset at just below 600 nm, indicating that these films possess a band gap of about 2.1 eV (Figure 2). The absorbance spectrum also possesses a shoulder at 540 nm and a peak at 400 nm, which are typical of α-Fe_2O_3 films and arise from indirect Fe^{3+} d to d and direct O^{2-} p to Fe^{3+} d transitions.[15]

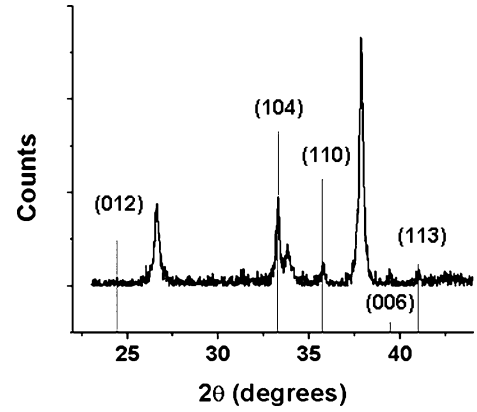

Figure 1. X-ray diffraction of an α-Fe_2O_3 film annealed in air for 2 h at 450 °C. Lines belonging to the hematite powder diffraction pattern are included. Other visible peaks are from the FTO substrate.

Electrochemical Impedance Spectroscopy. A film deposited at normal incidence (having little to no porosity) was analyzed to study the semiconducting properties of he-

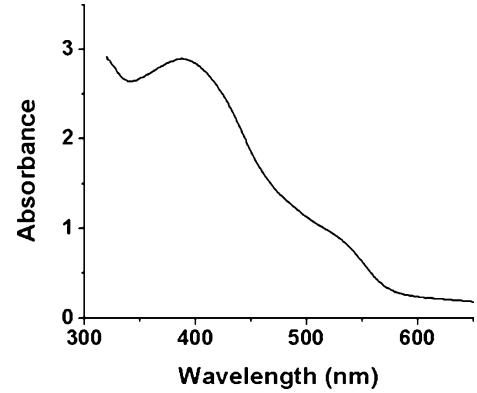

Figure 2. UV−vis absorbance of an α-Fe_2O_3 film approximately 200 nm thick annealed in air for 2 h at 450 °C.

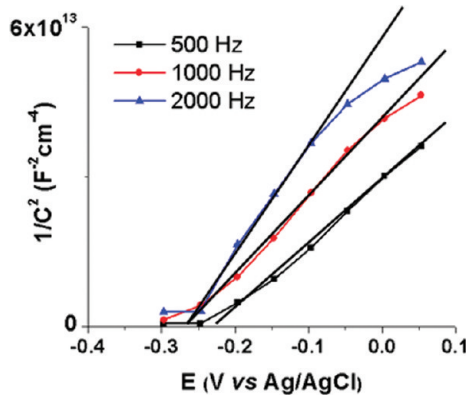

Figure 3. Mott−Schottky plots derived from electrochemical impedance spectroscopy performed at various frequencies and taken at pH 7 for a film deposited at 0° and annealed to 425 °C.

matite films prepared by our technique. Impedance spectroscopy was performed in pH 7 electrolyte using frequencies ranging from 500 to 2000 Hz and an AC amplitude of 10 mV at each potential. Some frequency dependence is observed, although the general behavior remains very similar over this frequency range. By taking the *x*-intercept of a linear fit to the Mott−Schottky plot for 1000 Hz (Figure 3), a flat-band potential of −0.27 V *versus* Ag/AgCl (−0.07 V *vs* NHE or +0.34 V *vs* the proton reduction potential at pH 7) was estimated, which agrees well with that expected for α-Fe_2O_3.[11] The Mott−Schottky slope was used, assuming a dielectric constant of 80,[32] to estimate a donor density of $\sim 10^{17}$ cm^{-3}. This is also in good agreement with literature values for single crystalline hematite electrodes[32,33] and indicates that the α-Fe_2O_3 films produced by RBD in this work possess the typically expected semiconducting properties of hematite.

Deposition Angle Effects. Glancing angle deposition techniques allow for control of thin film morphologies by taking advantage of ballistic shadowing and creating porous, columnar structures of the desired material. Such structures are thought to be necessary for achieving useful water splitting efficiencies with α-Fe_2O_3 thin films by creating a large film/electrolyte interfacial area and relatively short diffusion distances to this interface for holes generated within the bulk of the film by the absorption of photons, thus, improving the rate of charge transport relative to recombination. To investigate these effects various incident angles ranging from 0° (normal incidence) to 83° were used to deposit films of iron oxide, which were then annealed in air to produce crystalline hematite. Because bulk thickness is a critical factor in determining photoelectrochemical efficiency for α-Fe_2O_3 films, especially when effective dopants such as Si are not included,[34] multiple samples of different thicknesses were prepared at each deposition angle to clarify any trends in activity. Scanning electron microscopy (SEM) images revealed expected differences in morphology, with films deposited at normal incidence showing very little visible nanostructuring (essentially rough, dense films) and films deposited at glancing angles (>55°) showing more porous structures (Figure 4). This exemplifies the ballistic shadowing effect, which becomes more significant when glancing deposition angles and relatively low substrate temperatures are employed in a physical vapor deposition process.[25] Sections of films deposited at 55 and 82° were scraped off onto copper grids for transmission electron microscopy (TEM) analysis. The 82° deposition angle enabled examination of the surfaces of individual nanocolumns, whereas cross-sectional images of the 55° film appeared mostly dense at this level of resolution (Figure 5).

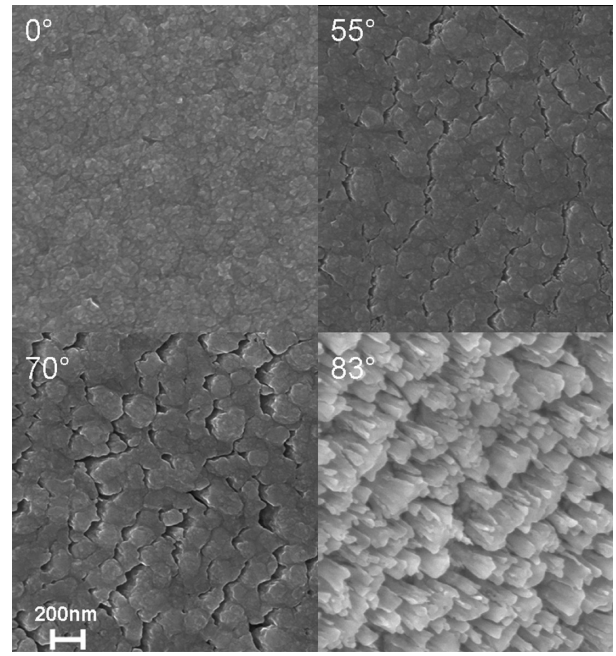

Figure 4. SEM images of α-Fe_2O_3 films deposited at various angles and annealed to 450 °C. The scale bar applies to all four images.

Films deposited at 55° consistently showed higher photocurrents under white light illumination than those deposited at other angles (the best performing films for each deposition angle are shown in Figure 6). This is a surprising result because it was expected that the more porous, nanocolumnar structures present in films deposited at more glancing angles would allow for easier hole transport to the electrolyte due to (theoretically) more optimal feature size and interfacial area. Additionally, preliminary results obtained from TiO_2 films deposited under very similar conditions in our laboratory showed highest photocurrents when deposited at 80°. It may be that the morphology of films deposited at high deposition angles is indeed better for hole transport, but other factors such as electron transport limitations and recombination centers act to mask this improvement in the case of α-Fe_2O_3. Films deposited at more glancing angles have greater porosity and conse-

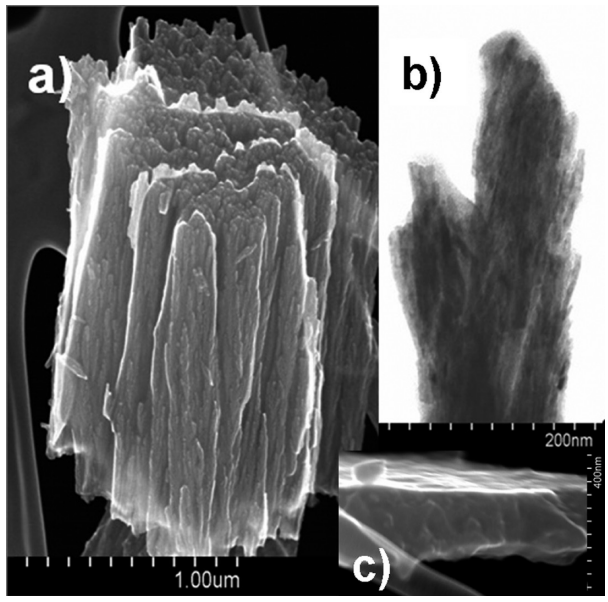

Figure 5. High resolution SEM image of a cluster of nanocolumns (a), and bright field TEM of the top of a single nanoclumn (b) from a film deposited at 82°. A high resolution SEM image of a cross-section of a film deposited at 55° is included (c) for comparison.

quently larger penetration depths (smaller photon absorption probability per unit thickness) than dense films, and photon absorption deeper in the film and close to the film−substrate interface is not desired because electrons and holes generated in this region are known to suffer from higher recombination rates due to factors that will be discussed more thoroughly below. For example, the penetration depths (α^{-1}) for 420 nm photons in films deposited at 55 and 80° are approximately 27 and 66 nm, respectively, based on UV−vis transmittance experiments. In a 150 nm thick film deposited at 55°, only 15% of the 420 nm photons are absorbed in the bottom 100 nm of the film, but in an equivalent film deposited at 80°, nearly 50% would be absorbed within the bottom 100 nm, revealing that many photons would be absorbed in a layer where their

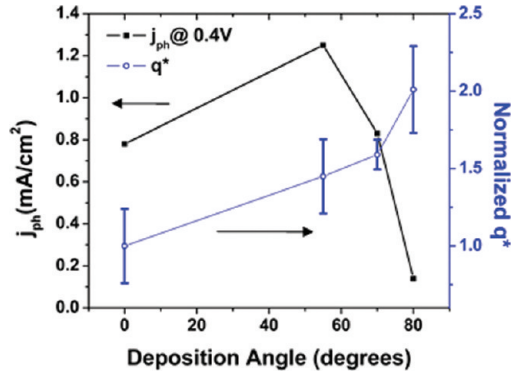

Figure 6. Optimized photocurrent values for films deposited at 0, 55, 70, and 80° plotted along with the total voltametric charge (q^*) transferred during CV sweeps between −0.1 and 0.1 V *vs* Ag/AgCl in 1 M KOH for films of similar thickness. All films were annealed at 450 °C for 2 h.

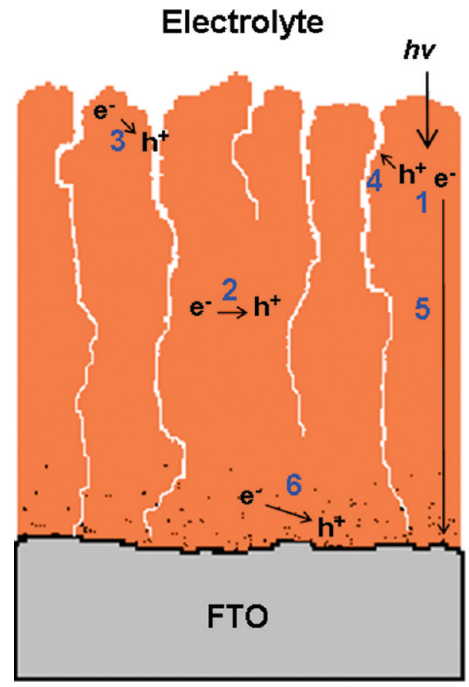

Figure 7. Schematic representation of processes occurring during irradiation of film: (1) light absorption and formation of electron−hole (e^-−h^+) pairs; (2) bulk recombination; (3) recombination at electrolyte interface; (4) hole transport; (5) electron transport; (6) recombination at the FTO interface.

probability of contributing to the photocurrent is significantly reduced. Although 100 nm is used in this example, the actual thickness and behavior of the "dead" layer is not well understood and probably depends on synthesis conditions as is investigated below. A seemingly obvious approach, then, for improving films deposited at 80° would be to significantly increase their thickness to keep so many photons from being absorbed near the FTO interface. However, now an appreciable amount of α-Fe_2O_3 lies between electrons generated near the top of the film and the external circuit, and the poor electronic conductivity of hematite leads to a low probability for these electrons to "complete the journey" before recombining with holes. These competing factors are illustrated in Figure 7 and may provide at least some explanation for the poor performance of high-porosity films deposited at angles above 70°, although the decrease in photocurrent as deposition angle is changed from 55 to 80° is clearly greater than what would be expected based on the preceding discussion, indicating that another or several factors, perhaps related to overall defect concentration, must be important also.

The specific surface areas of thin films deposited by RBD can vary widely as deposition angle is changed.[4,5] However, a better metric for evaluating thin films for PEC quality using materials with relatively poor charge transport properties like α-Fe_2O_3 may be surface area per unit thickness, because surface area improvements due to increased film thickness are not beneficial.[22]

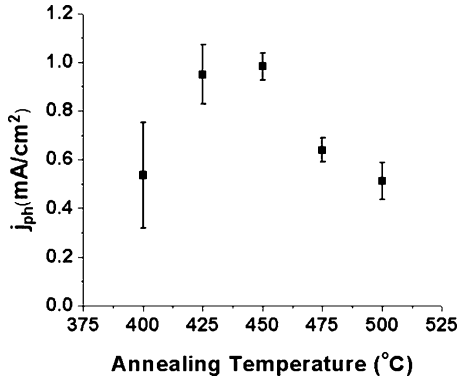

Figure 8. Photocurrent trend at 0.4 V *vs* Ag/AgCl as annealing temperature is increased for films deposited at 55° and having thicknesses of ~240 nm.

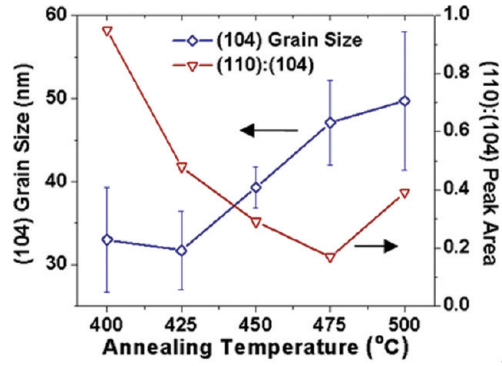

Figure 9. Mean crystallite size of the (104) plane and ratio of the integrated XRD peak areas for the (110) and (104) planes plotted for different annealing temperatures.

Films of approximately equal thickness (180 nm) but deposited at different angles (0, 55, 70, and 80°) were evaluated using cyclic voltammetry (CV). The total voltammetric charge produced on the surface and in the electrolyte during a potential scan in which only capacitive charge transfer occurs is proportional the number of available surface sites.[35] Integration of the charge during potential cycles from −0.1 to 0.1 V *versus* Ag/AgCl in 1 M KOH at 20 mVs^{-1} performed on films in the dark indicated that surface area doubled as the deposition angle increased from 0 to 80° when films of approximately equal thickness were compared (Figure 6). Note that the surface area of α-Fe_2O_3 *per unit mass* actually increased by nearly a factor of 6 over this range. For the case of the more porous films there may be some small error introduced due to a contribution from exposed FTO substrate with the electrolyte. Although 80° showed the highest surface area of the deposition angles tested, it is unknown whether higher deposition angles would result in even larger surface areas. Various groups have shown that the deposition angle corresponding to greatest surface area for ballistically deposited films is not the same for all materials (*i.e.*, TiO_2 shows a maximum at 70°,[4] while Pd shows a maximum at 85°[29]). A high surface area per unit film thickness would theoretically be advantageous for PEC water splitting because it implies that a significant fraction of the holes generated in the film will be created near the interface between the film and the electrolyte, minimizing their required transport distance. However, in this study there does not appear to be a strong correlation between available surface area (on a film thickness basis) and photocurrent for the more porous films (Figure 6), indicating that other factors such as electron transport limit the PEC performance of films deposited at glancing angles.

Annealing Temperature and Bulk Thickness Effects. Films with thicknesses of ~240 nm were deposited at 55° and annealed for 2 h in air at temperatures ranging from 400 to 500 °C to investigate the sensitivity of PEC performance to postdeposition heat treatment (Figure 8). A significant increase in photocurrent was observed as the annealing temperature increased from 400 to 425 and 450 °C, followed by a noticeable decrease for samples annealed beyond 450 °C. The expected reason for the initial rise in photocurrent with annealing temperature is the improvement of crystalline order and reduction of defects within the film. This should theoretically improve charge carrier transport relative to recombination, which is a strong limiting determining factor in the PEC performance in undoped α-Fe_2O_3 films. Most peaks in the XRD spectrum belonging to α-Fe_2O_3, particularly the (104) plane, show a marked increase in intensity relative to the SnO_2 peaks as the annealing temperature increased from 425 to 500 °C, indicating a general improvement in crystalline character of the α-Fe_2O_3 film. The Scherrer equation was used to calculate the mean grain size of the (104) plane for films at each annealing temperature (Figure 9). As expected, the mean (104) grain size generally grows with increasing temperature, increasing from 33 to 50 nm over the range of annealing temperatures studied. However, this is not observed between 400 and 425 °C. In fact, the only obvious difference between 400 and 425 °C annealed films appears to be a *decrease* in (110) orientation relative to other planes (Figure 9). That this change

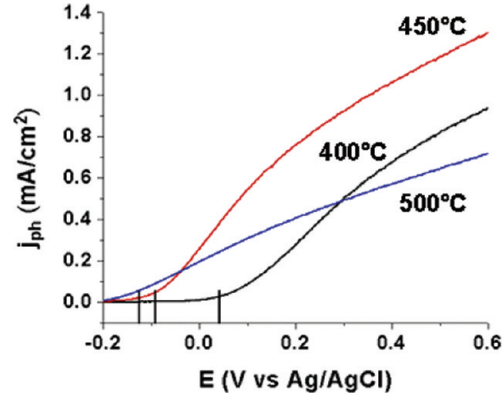

Figure 10. Photoelectrochemical behavior under white-light illumination in 1 M KOH for films annealed to various temperatures. The photocurrent onset potentials (vertical lines) tended to shift negatively as temperature increased.

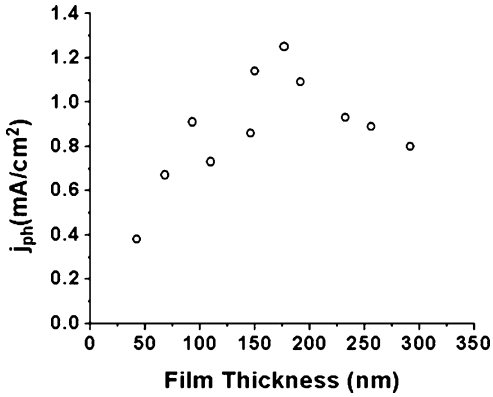

Figure 11. Steady state photocurrent at 0.4 V *vs* Ag/AgCl in 1 M KOH for a variety of film thicknesses. Films were deposited at 55° and annealed to 450 °C for 2 h.

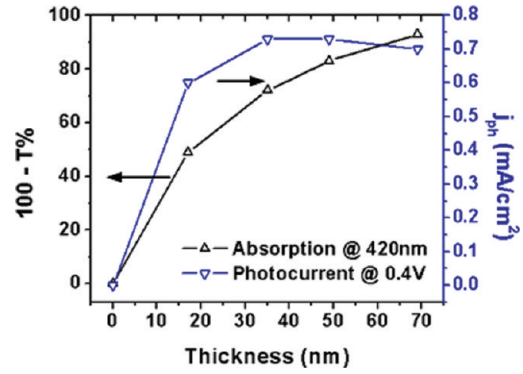

Figure 12. Comparison of photocurrent at 0.4 V *vs* Ag/AgCl and photon absorption at 420 nm trends for very thin films annealed to 550 °C.

is accompanied by a strong *increase* in photocurrent is surprising because a preferred (110) orientation is thought to be beneficial to vertical electron transport within α-Fe_2O_3 films due to the anisotropic conductivity of hematite, although this orientation may not be as important as other factors.[12,14] It is quite possible that an increase in annealing temperature from 400 to 425 °C reduces the number of defects in the film, but in a way, that is not easily detectable by XRD, and this is responsible for the improvement in photocurrent over this range.

Although changes in crystallinity and defect concentration are likely explanations for the initial rise in photocurrent from 400 to 450 °C, they do not explain the significant drop in photocurrent as the annealing temperature increases from 450 to 500 °C. Because fine, nanoscale features provide improved transport to the film−electrolyte interface for holes photogenerated within the film, the agglomeration of these features and corresponding increase in hole transport distance is the most likely explanation for the decrease in performance from 450 to 500 °C, although voltammetric charge integration experiments performed on films annealed over this temperature range do not show significant changes in surface area. This method may not be precise enough to elucidate such subtle differences. Surprisingly, the decrease in performance at higher annealing temperatures is not observed for extremely thin films since the limiting factor in their performance appears to be recombination due to defects near the film−FTO interface rather than poor hole transport due to feature size differences brought about by annealing. Additionally, SEM images of the thinnest films indicate that these have a more open structure with Fe_2O_3 preferentially depositing on the peaks of the rough FTO substrate layer. In the thin film case, deposition was halted before these deposits could thicken and grow together as they normally would when employing a 55° deposition angle, causing their morphology to be somewhat different than that of the thicker films even though all other conditions are held constant.

Although photocurrent decreased when annealing temperatures increased above 450 °C, a noticeable negative shift in the photocurrent onset potential was also observed (Figure 10). The trends in both peak photocurrent and photocurrent onset are very similar to those observed by Cesar *et al.* for Si-doped films prepared by CVD[34] and annealed from temperatures ranging from 450 to 490 °C. The shift in photocurrent onset was attributed to a decrease in recombination on the α-Fe_2O_3 surface, which could be due to differences in surface area and the nature of surface sites. Temperature programmed desorption studies performed on MgO films[3] and others produced by RBD indicate that the surface site distribution on such materials can be manipulated through annealing, although it is not clear whether this effect would be significant over the annealing temperature range studied here. It may be that the sites prevalent on α-Fe_2O_3 surfaces in the case of the lower temperature films are somehow less effective from the point of view of charge transfer or recombination or the observed effects could be entirely due to a decrease in surface area, as previously suggested.[34]

A number of films were deposited at 55° with varying thicknesses in order to study the effects of film thickness on photocurrent performance. Increasing thickness allows for greater light absorption but decreases electron extraction efficiency in α-Fe_2O_3 due to poor electron transport over such distances. Indeed, the observed trend of photocurrent performance shows a volcano-like dependence on film thickness (Figure 11). However, the observed performance trend for very thin films annealed to 450 °C does not match the corresponding photon absorbance trend. For films less than 150 nm thick the photocurrent drops off quite rapidly despite the fact that these films still absorb over 90% of the available photons in the incident light. Put another way, even the *absorbed* photon to current conversion efficiency (APCE) must be much lower for the thinner films, which is somewhat counterintuitive since one would expect electrons generated near the surface of

a thinner film to have a higher probability of reaching the back contact if all other factors remained constant. Clearly the increase in photocurrent observed as film thickness is increased to ~180 nm is not solely due to improved photon absorption, but may be more related to the fact that most of the electrons and holes are not generated adjacent to the film−FTO interface, because it has been suggested that charge carriers generated near this interface suffer from higher recombination rates.[34,36,37] If few photons are absorbed in this region, as is the case for thicker films, then only majority carriers (electrons) are present near the film−FTO interface as they pass through to the back contact. Because minority carrier (hole) concentrations should be low near the interface in thick films, recombination would not be as problematic.

One possible reason put forth for this is the extension of electrons from the FTO substrate into the bottom layers of the α-Fe_2O_3 film,[36] although this effect would likely be limited to a small fraction of even the thinnest films investigated here. A more probable cause of excessive electron−hole recombination near the film−FTO interface could be crystal defects (amorphous regions, grain boundaries, strain effects, *etc.*) acting as recombination centers in the region.[34] It has been suggested that intermediate energy levels in α-Fe_2O_3 can be formed due to stress near the film−FTO interface and resultant lattice defects, which are then associated with electron trapping and higher recombination rates.[37] Extremely thin films (18−70 nm) were deposited and annealed to higher temperatures (500−550 °C) in an attempt to improve the crystalline order near the film−substrate interface. The thicknesses of these thin films were estimated by depositing thick films (which could be more easily measured), calculating their resulting film thicknesses as functions of deposited Fe mass and using this relationship to calculate the thicknesses of thinner films prepared by depositing a known mass of Fe. However, shadowing due to the roughness of the FTO substrate causes these thin films to possess larger void fractions and be somewhat thicker than what is calculated by this method. Interestingly enough, the films annealed to higher temperatures (greater than 450 °C) show much better photoactivity than the films of similar thickness annealed to 450 °C, in stark contrast to the behavior of thicker films. Films annealed to 450 °C show quite different activity−thickness trends compared to those annealed to 550 °C, with the photocurrents of the former films leveling off at thicknesses of 180 nm, compared to only 35 nm in the latter case (Figure 12). The trend in performance of the films annealed to 550 °C seems to match the optical absorption trend much more closely for small film thicknesses, indicating that recombination near the film-FTO interface has been suppressed relative to that in films annealed to 450 °C. IPCE experiments using both front and backside illumination were performed on films deposited at

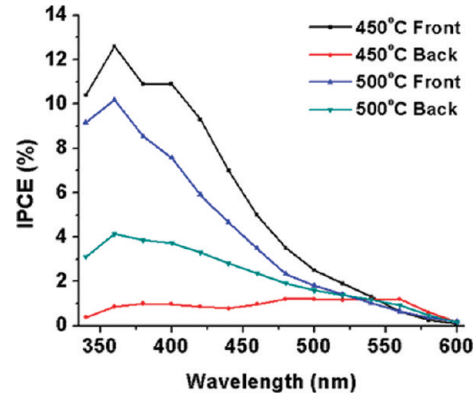

Figure 13. IPCE spectra for front and backside illumination for films deposited at 55° incidence and annealed to 450 or 500 °C for 2 h. The experiments were performed in 1 M KOH using an applied potential of +0.5 V *vs* Ag/AgCl.

55° incidence (~240 nm thick) and annealed to either 450 or 500 °C (Figure 13). For front-side experiments, a blank substrate was attached to the front of the electrochemical cell to mimic the transmittance loss that would occur in the back-side illumination experiments. While films annealed to 450 °C showed drastically diminished photoconversion, especially for higher energy photons, the films annealed to 500 °C showed a much less precipitous drop in photoactivity when back-side illumination was employed. The preferential recombination of higher-energy photons can be easily explained because their penetration depths are much shorter and are thus absorbed nearer the film−FTO interface. Although clear improvements in the photoconversion of photons absorbed near the film−FTO interface were achieved using annealing temperatures higher than 450 °C, the best performing films overall using front-side illumination were thicker films annealed to 450 °C.

Photoconversion Performance. Films deposited using seemingly optimum conditions (55° deposition angle, 180 nm thick, 450 °C annealing for 2 h) were assessed using incident photon conversion efficiency (IPCE) calculations at wavelengths ranging from 350 to 600 nm at a potential of +0.5 V *versus* Ag/AgCl (Figure 14), which is just below the onset of noticeable dark electrolysis

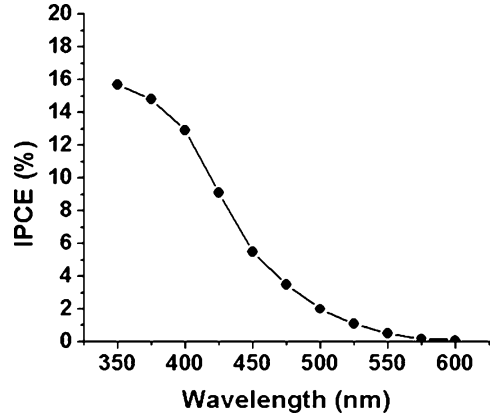

Figure 14. IPCE spectrum of an optimized film recorded in 1 M KOH at +0.5 V *vs* Ag/AgCl.

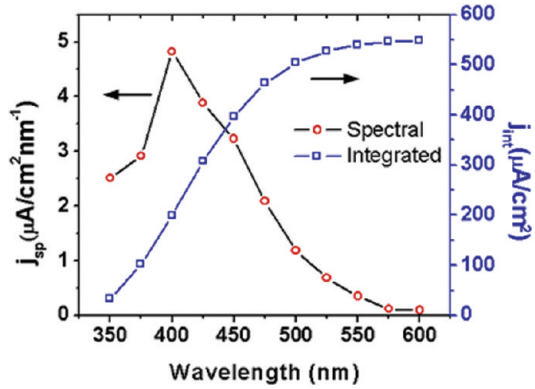

Figure 15. Spectral photocurrent data under AM1.5 illumination calculated from IPCE data at +0.5 V *vs* Ag/AgCl.

current in 1 M KOH. When integrated over the AM1.5 solar spectrum[38] the IPCE data results in a solar photocurrent density of 549 $\mu A/cm^2$ (Figure 15), which is less than half of the white-light photocurrent measured under the Xe lamp irradiation used in these experiments (Figure 16) due to the higher intensity of the lamp illumination at the sample relative to AM1.5 as well as to the spectral mismatch between the two sources. Additionally, the filling of trap states by photons of a wide range of energies available under white-light illumination may allow for greater charge carrier mobility and thus contribute to a higher photocurrent compared to the case in which monochromatic illumination is used. The photocurrent values achieved in this study are reasonable when compared with literature values for undoped α-Fe_2O_3 prepared by various methods with most showing values in the several hundred $\mu A/cm^2$ range under AM1.5 illumination,[15] although IPCE values are often not reported. The highest IPCE values reported so far for undoped α-Fe_2O_3 films appear to belong to films prepared by spray pyrolysis with a peak IPCE of just over 20% in the UV range[14,16] compared to 15% found in this study under similar conditions. Films tested for 10 to 15 min under constant illumination showed very little (~1%) decrease in photocurrent, and the accumulation of small bubbles could be observed on the film surface, indicating that the photocurrent is due to oxygen evolution rather than photocorrosion of the film.

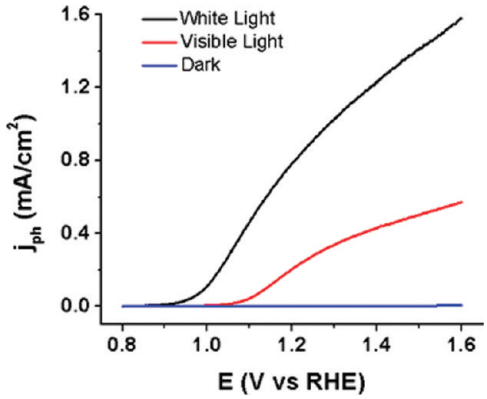

Figure 16. Current−potential plots in 1 M KOH in the dark and under white and visible (>420 nm) light plotted against the reversible hydrogen electrode. The film was deposited at 55° and 180 nm thick and annealed for 2 h at 450 °C.

The rapid drop-off in quantum yield beyond 400−420 nm has been noted by many authors and seems to occur regardless of the technique used to prepare the α-Fe_2O_3 thin film.[34,36,39] This is a significant problem with regard to achieving practical water splitting efficiencies under solar irradiation because the bulk of the photons available to α-Fe_2O_3 lie in the 450−585 nm range. One possible reason for this behavior is the larger penetration depths of lower energy photons in hematite, as evidenced by the UV−vis absorption spectrum, which possesses a similar shape to the IPCE spectrum. Holes generated by these photons in planar electrodes are less likely to reach the film−electrolyte interface before recombination because of the notoriously low hole diffusion distance in undoped α-Fe_2O_3 of 2−4 nm.[39] Nanoporous or nanocolumnar materials consisting of structures that closely match this hole diffusion length have been proposed to alleviate such problems, but in practice, this strategy does not seem to significantly alter the shape of the IPCE spectrum for α-Fe_2O_3 films.[34] This implies that holes generated by low energy photons are somehow less inherently efficient for water oxidation than those generated by high energy photons in α-Fe_2O_3. The reasons for this are unclear, especially considering that holes generated in the O_{2p} band should seemingly relax to the lowest energy states available in the valence band (the top of the Fe_{3d} band) prior to participating in any processes at the surface of the electrode.[40] It has been hypothesized that holes created at Fe^{3+} sites are somehow less available for water oxidation than those created at O^{2-} sites, resulting in a weaker contribution to the photocurrent.[39]

CONCLUSIONS

We have reported on the use of a novel technique known as reactive ballistic deposition (RBD) for preparing and optimizing α-Fe_2O_3 thin films on FTO substrates for water splitting applications. By manipulating parameters, such as film thickness, morphology, and crystallinity, it is possible to tune the PEC properties of potentially interesting materials for the photo-oxidation of water, such as α-Fe_2O_3. Changing the angle of deposition between 0 and 83° resulted in substantial morphological differences between the films, which played a strong role in determining their PEC performance and incident photon to current conversion efficiencies (IPCE). Various film thicknesses and annealing temperatures were also investigated to determine the optimum film synthesis conditions. Films approximately 180 nm thick, deposited at 55° incidence and annealed to 450 °C, show the highest photocurrents of those studied here for the photo-oxidation of water in 1 M KOH under Xe lamp illumination. These synthesis conditions appear to balance competing effects related to

photon absorption, charge carrier transport and recombination in α-Fe_2O_3 films. The optimized films of undoped α-Fe_2O_3 in this study show good performance with photocurrents exceeding 0.5 mA/cm^2 under solar illumination, as calculated by integration of the IPCE values over the AM1.5 spectrum.

METHODS

Film Preparation. Hematite films were deposited onto fluorine-doped tin oxide (FTO) coated glass substrates (Pilkington, TEC15) held at room temperature by evaporating Fe metal in a background of O_2 under high vacuum conditions ($\sim 10^{-6}$ Torr). The vacuum chamber was first pumped down to below 5×10^{-8} Torr and then backfilled to approximately 1×10^{-6} Torr with O_2 (99.99%, Matheson) using a leak valve (the majority of the remaining background is H_2O). This level of backfilling was found to be well in excess of the amount required to fully oxidize the films based on quartz crystal microbalance uptake measurements. Iron was evaporated from a 0.25" diameter rod (3N5 purity, ESPI) using an electron-beam evaporator (Tectra). The substrate holder could be rotated, allowing for utilization of the entire possible range of deposition angles (0−90°), and the source to substrate distance was approximately 10 cm. After deposition the samples were annealed in air at temperatures ranging from 400 to 550 °C for 2 h in a box furnace (Neytech). The temperature was brought from room temperature to the desired annealing temperature at a rate of 10 °C/min, and the samples were allowed to cool naturally after the desired hold time was reached.

Film Characterization. SEM was performed on a LEO 1530 SEM using a 10 kV focus voltage and on a Hitachi S-5500 scanning transmission electron microscope (STEM) using a 30 kV focus voltage. The Hitachi S-5500 was also used to perform EDS and TEM. XRD experiments utilized a Phillips diffractometer. UV−vis transmission spectra were taken with a Cary 5000 spectrophotometer using a blank substrate as a baseline standard. Optical penetration depths (α^{-1}) were calculated using

$$\alpha^{-1} = D/(-\ln(T)) \quad (1)$$

Here, α is the absorption coefficient, D is the thickness of the film, and T is the measured transmittance. Therefore, α^{-1} is the distance over which photons of the wavelength of interest are attenuated to an intensity equal to their original intensity multiplied by $1/e(0.368)$. XPS was performed using a Kratos AXIS X-ray photoelectron spectrometer.

Electrochemical Testing. The electrochemical and photoelectrochemical properties of each sample were tested using a three-electrode electrochemical cell with a Ag/AgCl reference electrode and Pt mesh counterelectrode. The working electrode (the photoanode consisting of the α-Fe_2O_3 film) with illuminated area 0.21 cm^2 was immersed in 1 M KOH and illuminated using an unfiltered 150 W xenon lamp (Oriel) with a white-light intensity of $\sim$130 mW/cm^2. A monochromator (Oriel) was also employed to study spectral response and was used in conjunction with a power meter and photodiode (Newport) to calculate IPCE, given by

$$\mathrm{IPCE} = [1240 \times j_{ph}/(\lambda \times I)] \times 100\% \quad (2)$$

Here, j_{ph} is the steady state photocurrent density, λ is the wavelength of the incident light, and I is the light power intensity at the film surface. A potentiostat (CH Instruments) was operated by a desktop computer to perform electrochemical measurements. Steady-state photocurrents for comparing the films to one another were recorded at +0.4 V *versus* Ag/AgCl, whereas IPCE experiments were performed at +0.5 V to maximize the ratio of illuminated current to dark current (dark currents began to increase beyond +0.5 V). Electrochemical impedance spectroscopy was performed using a Solartron frequency response analyzer and electrochemical interface system. Plots of inverse square capacitance C^{-2} ($1/C^2$) *versus* potential (E) can be used to determine the flat-band potential (E_{fb}) and donor density (N_d) of n-type semiconductor films using the Mott−Schottky equation:

$$1/C^2 = [2/(e\varepsilon\varepsilon_o N_d)](E - E_{fb} - kT/e) \quad (3)$$

Here, e is the elementary charge, ε is the dielectric constant of the electrode material, ε_o is the permittivity of vacuum, and C is the capacitance of the electrode. The x-intercept of a linear fit to a plot of C^{-2} ($1/C^2$) *versus* E reveals the flat-band potential, while the slope of this fit can be used to calculate N_d.

Acknowledgment. C.B.M. and A.J.B. gratefully acknowledge the support of the National Science Foundation (CHE-0934450). Additionally, this work has been partially supported by the U.S. Army Research Laboratory and the U.S. Army Research Office (for C.B.M. under Contract/Grant Number W911NF-09-1-0130) and the Welch Foundation (for C.B.M. under Grant Number F-1436). A.J.B. also acknowledges the Welch Foundation (F-0021) for their generous support. C.B.M. and A.J.B. also acknowledge the National Science Foundation (Grant No. 0618242) for funding the X-ray Photoelectron Spectrometer used in this work. Finally, we also thank the reviewers for their thoughtful and insightful comments.

Supporting Information Available: XPS data (as noted in the text) and an SEM image of an additional film. This material is available free of charge *via* the Internet at http://pubs.acs.org.

REFERENCES AND NOTES

1. Fujishima, A.; Honda, K. Electrochemical Photolysis of Water at a Semiconductor Electrode. *Nature* **1972**, *238*, 37–38.
2. Lewis, N.; Crabtree, G. *Basic Research Needs for Solar Energy Utilization*; U.S. Department of Energy: Washington, DC, 2005.
3. Dohnalek, Z.; Kimmel, G. A.; McCready, D. E.; Young, J. S.; Dohnalkova, A.; Smith, R. S.; Kay, B. D. Structural and Chemical Characterization of Aligned Crystalline Nanoporous MgO Films Grown via Reactive Ballistic Deposition. *J. Phys. Chem. B* **2002**, *106*, 3526–3529.
4. Flaherty, D. W.; Dohnalek, Z.; Dohnalkova, A.; Arey, B. W.; McCready, D. E.; Ponnusamy, N.; Mullins, C. B.; Kay, B. D. Reactive Ballistic Deposition of Porous TiO_2 Films: Growth and Characterization. *J. Phys. Chem. C* **2007**, *111*, 4765–4773.
5. Flaherty, D. W.; Hahn, N. T.; Ferrer, D.; Engstrom, T. R.; Tanaka, P. L.; Mullins, C. B. Growth and Characterization of High Surface Area Titanium Carbide. *J. Phys. Chem. C* **2009**, *113*, 12742–12752.
6. Flaherty, D. W.; May, R. A.; Berglund, S. P.; Stevenson, K. J.; Mullins, C. B. Low Temperature Synthesis and Characterization of Nanocrystalline Titanium Carbide With Tunable Porous Architectures. *Chem. Mater.* **2010**, *22*, 319–329.
7. van de Krol, R.; Liang, Y. Q.; Schoonman, J. Solar Hydrogen Production with Nanostructured Metal Oxides. *J. Mater. Chem.* **2008**, *18*, 2311–2320.
8. Shankar, K.; Basham, J. I.; Allam, N. K.; Varghese, O. K.; Mor, G. K.; Feng, X. J.; Paulose, M.; Seabold, J. A.; Choi, K. S.; Grimes, C. A. Recent Advances in the Use of TiO_2 Nanotube and Nanowire Arrays for Oxidative Photoelectrochemistry. *J. Phys. Chem. C* **2009**, *113*, 6327–6359.
9. Park, J. H.; Kim, S.; Bard, A. J. Novel Carbon-Doped TiO_2 Nanotube Arrays With High Aspect Ratios for Efficient Solar Water Splitting. *Nano Lett.* **2006**, *6*, 24–28.

10. Bard, A. J.; Fox, M. A. Artificial Photosynthesis: Solar Splitting of Water to Hydrogen and Oxygen. *Acc. Chem. Res.* **1995**, *28*, 141–145.
11. Murphy, A. B.; Barnes, P. R. F.; Randeniya, L. K.; Plumb, I. C.; Grey, I. E.; Horne, M. D.; Glasscock, J. A. Efficiency of Solar Water Splitting Using Semiconductor Electrodes. *Int. J. Hydrogen Energy* **2006**, *31*, 1999–2017.
12. Kay, A.; Cesar, I.; Gratzel, M. New Benchmark for Water Photooxidation by Nanostructured α-Fe_2O_3 Films. *J. Am. Chem. Soc.* **2006**, *128*, 15714–15721.
13. Lindgren, T.; Vayssieres, L.; Wang, H.; Lindquist, S. E. Photo-Oxidation of Water at Hematite Electrodes. In *Chemical Physics of Nanostructured Semiconductors*; Bahnemann, D. W., Ed.; VSP: Utrecht, 2003; 83−110.
14. Glasscock, J. A.; Barnes, P. R. F.; Plumb, I. C.; Savvides, N. Enhancement of Photoelectrochemical Hydrogen Production from Hematite Thin Films by the Introduction of Ti and Si. *J. Phys. Chem. C* **2007**, *111*, 16477–16488.
15. Jang, J. S.; Lee, J.; Ye, H.; Fan, F. R. F.; Bard, A. J. Rapid Screening of Effective Dopants for Fe_2O_3 Photocatalysts with Scanning Electrochemical Microscopy and Investigation of their Photoelectrochemical Properties. *J. Phys. Chem. C* **2009**, *113*, 6719–6724.
16. Hu, Y. S.; Kleiman-Shwarsctein, A.; Forman, A. J.; Hazen, D.; Park, J. N.; McFarland, E. W. Pt-doped α-Fe_2O_3 Thin Films Active for Photoelectrochemical Water Splitting. *Chem. Mater.* **2008**, *20*, 3803–3805.
17. Sartoretti, C. J.; Alexander, B. D.; Solarska, R.; Rutkowska, W. A.; Augustynski, J.; Cerny, R. Photoelectrochemical Oxidation of Water at Transparent Ferric Oxide Film Electrodes. *J. Phys. Chem. B* **2005**, *109*, 13685–13692.
18. Duret, A.; Gratzel, M. Visible Light-Induced Water Oxidation on Mesoscopic α-Fe_2O_3 Films Made by Ultrasonic Spray Pyrolysis. *J. Phys. Chem. B* **2005**, *109*, 17184–17191.
19. Khan, S. U. M.; Akikusa, J. Photoelectrochemical Splitting of Water at Nanocrystalline n-Fe_2O_3 Thin-Film Electrodes. *J. Phys. Chem. B* **1999**, *103*, 7184–7189.
20. Hardee, K. L.; Bard, A. J. Semiconductor Electrodes. V. The Application of Chemically Vapor Deposited Iron Oxide Films to Photosensitized Electrolysis. *J. Electrochem. Soc.* **1976**, *123*, 1024–1026.
21. Kleiman-Shwarsctein, A.; Hu, Y. S.; Forman, A. J.; Stucky, G. D.; McFarland, E. W. Electrodeposition of α-Fe_2O_3 Doped with Mo or Cr as Photoanodes for Photocatalytic Water Splitting. *J. Phys. Chem. C* **2008**, *112*, 15900–15907.
22. Spray, R. L.; Choi, K. S. Photoactivity of Transparent Nanocrystalline Fe_2O_3 Electrodes Prepared via Anodic Electrodeposition. *Chem. Mater.* **2009**, *21*, 3701–3709.
23. LaTempa, T. J.; Feng, X. J.; Paulose, M.; Grimes, C. A. Temperature-Dependent Growth of Self-Assembled Hematite (α-Fe_2O_3) Nanotube Arrays: Rapid Electrochemical Synthesis and Photoelectrochemical Properties. *J. Phys. Chem. C* **2009**, *113*, 16293–16298.
24. Mohapatra, S. K.; John, S. E.; Banerjee, S.; Misra, M. Water Photooxidation by Smooth and Ultrathin α-Fe_2O_3 Nanotube Arrays. *Chem. Mater.* **2009**, *21*, 3048–3055.
25. Hawkeye, M. M.; Brett, M. J. Glancing Angle Deposition: Fabrication, Properties, and Applications of Micro- and Nanostructured Thin Films. *J. Vac. Sci. Technol., A* **2007**, *25*, 1317–1335.
26. Xi, J. Q.; Schubert, M. F.; Kim, J. K.; Schubert, E. F.; Chen, M. F.; Lin, S. Y.; Liu, W.; Smart, J. A. Optical Thin-Film Materials with Low Refractive Index for Broadband Elimination of Fresnel Reflection. *Nat. Photonics* **2007**, *1*, 176–179.
27. Robbie, K.; Brett, M. J.; Lakhtakia, A. Chiral Sculptured Thin Films. *Nature* **1996**, *384*, 616.
28. Kim, J. K.; Chhajed, S.; Schubert, M. F.; Schubert, E. F.; Fischer, A. J.; Crawford, M. H.; Cho, J.; Kim, H.; Sone, C. Light-Extraction Enhancement of GaInN Light-Emitting Diodes by Graded-Refractive-Index Indium Tin Oxide Anti-Reflection Contact. *Adv. Mater.* **2008**, *20*, 801–804.
29. Kim, J.; Dohnalek, Z.; Kay, B. D. Structural Characterization of Nanoporous Pd Films Grown via Ballistic Deposition. *Surf. Sci.* **2005**, *586*, 137–145.
30. Wolcott, A.; Smith, W. A.; Kuykendall, T. R.; Zhao, Y. P.; Zhang, J. Z. Photoelectrochemical Water Splitting Using Dense and Aligned TiO_2 Nanorod Arrays. *Small* **2009**, *5*, 104–111.
31. Wolcott, A.; Smith, W. A.; Kuykendall, T. R.; Zhao, Y. P.; Zhang, J. Z. Photoelectrochemical Study of Nanostructured ZnO Thin Films for Hydrogen Generation from Water Splitting. *Adv. Funct. Mater.* **2009**, *19*, 1849–1856.
32. Kennedy, J. H.; Frese, K. W. Flatband Potentials and Donor Densities of Polycrystalline α-Fe_2O_3 Determined from Mott−Schottky Plots. *J. Electrochem. Soc.* **1978**, *125*, 723–726.
33. Eggleston, C. M.; Shankle, A. J. A.; Moyer, A. J.; Cesar, I.; Gratzel, M. Anisotropic Photocatalytic Properties of Hematite. *Aquat. Sci.* **2009**, *71*, 151–159.
34. Cesar, I.; Sivula, K.; Kay, A.; Zboril, R.; Graetzel, M. Influence of Feature Size, Film Thickness, and Silicon Doping on the Performance of Nanostructured Hematite Photoanodes for Solar Water Splitting. *J. Phys. Chem. C* **2009**, *113*, 772–782.
35. Spinolo, G.; Ardizzone, S.; Trasatti, S. Surface Characterization of Co_3O_4 Electrodes Prepared by the Sol-Gel Method. *J. Electroanal. Chem.* **1997**, *423*, 49–57.
36. Itoh, K.; Bockris, J. O. Thin-Film Photoelectrochemistry: Iron-Oxide. *J. Electrochem. Soc.* **1984**, *131*, 1266–1271.
37. Souza, F. L.; Lopes, K. P.; Longo, E.; Leite, E. R. The Influence of the Film Thickness of Nanostructured α-Fe_2O_3 on Water Photooxidation. *Phys. Chem. Chem. Phys.* **2009**, *11*, 1215–1219.
38. NREL AM 1.5 Gobal solar spectrum derived from SMARTS v.2.9.2; http://rredc.nrel.gov/solar/spectra/am1.5/.
39. Kennedy, J. H.; Frese, K. W. Photooxidation of Water at α-Fe_2O_3 Electrodes. *J. Electrochem. Soc.* **1977**, *125*, 709–714.
40. Nozik, A. J.; Memming, R. Physical Chemistry of Semiconductor−Liquid Interfaces. *J. Phys. Chem.* **1996**, *100*, 13061–13078.